Effects on UV line observations of stationary plasma flows confined in coronal loops

S. Orlando[1,2] and G. Peres[2]

[1]ESA Solar System Division, Space Science Dept., ESTEC, Noordwijk, The Netherlands
[2]Dip. di Scienze Fis. ed Astr. - Sezione di Astronomia - Univ. di Palermo, Palermo, Italy

Camera-ready Copy for

Physics and Chemistry of the Earth

Manuscript-No. ST13.01-0010

Offset requests to:
S. Orlando
SCI-SO, ESA-ESTEC
Noordwijk, The Netherlands

Effects on UV line observations of stationary plasma flows confined in coronal loops

S. Orlando[1,2] **and G. Peres**[2]

[1]ESA Solar System Division, Space Science Dept., ESTEC, Noordwijk, The Netherlands
[2]Dip. di Scienze Fis. ed Astr. - Sezione di Astronomia - Univ. di Palermo, Palermo, Italy

Received – Accepted

Abstract. We describe a method which uses a rather detailed model of coronal loop hosting a siphon flow as a diagnostic tool to interpret solar UV and X–ray observations in selected bands and lines. We apply the method to investigate the deviations from ionization equilibrium induced by stationary plasma flows confined in coronal loops and their effects on the UV and EUV emission lines observed by the instruments on board SOHO. We present results on the detailed synthesis of loop emission in a set of selected emission lines observed by CDS and SUMER, taking into account the non–equilibrium of ionization effects.

1 Introduction

As shown by observations with rockets and satellites over approximately three decades, the solar corona is highly structured by the magnetic field which confines the hot plasma into bright loops anchored in the chromosphere. The energetics and the dynamics of the chromosphere and the corona were investigated through the accurate analysis of the loops morphology, and of the physical conditions of the plasma therein confined. In particular, the analysis of emission lines forming at temperatures ranging from the chromosphere up to the corona gives important information on the temperature and density stratification inside each individual loop.

In the present context, mostly dedicated to loops which undergo only slow evolution with respect with their typical cooling time, the analysis mentioned above can be important to understand the physical conditions of the plasma confined in loops outside transient phenomena, such as flares. For instance, since in general coronal loops connect two different regions of the solar surface where the physical conditions can be significantly different, one can expect to observe significant asymmetry of the two footpoints and part of the loop's legs. Through the analysis of the loop asymmetry we may, therefore, constrain the physical mechanisms conducive to the conditions of the loop plasma. For example, the plasma pressure or the volumetric heating can be different at the two footpoints and could drive a significant plasma flow (siphon flow) along the loop making the whole structure and its emission in EUV lines significantly asymmetric. In this particular case, the detection of possible asymmetries may be the key to show or to exclude evidence of a siphon flow and/or different heating conditions between the two loop footpoints.

The above considerations are particularly important in the light of the high spatial and spectral resolution of the spectroscopic instruments on board the Solar and Heliospheric Observatory (SOHO), most notably CDS (*Coronal Diagnostic Spectrometer*) and SUMER (*Solar Ultraviolet Measurements of Emitted radiation*). Such instruments have observed, to a high degree of accuracy, spectral lines forming in different layers of the solar atmosphere acquiring a continuous sequence of daily EUV and X–ray solar data during the solar–cycle minimum and providing, therefore, an high quality data archive to investigate the physical conditions of the emitted plasma confined into the loops. In fact, the analysis of such data is giving a new and deep insight into the solar loop physics, complementary to that provided by the instruments on board Yohkoh.

On the other hand, the energetics and the dynamics of the loop plasma are quite complex with several important mechanisms of comparable importance and non–linear behaviour, such as the heat conduction and the radiative losses mechanism, simultaneously at work. As a consequence, the interpretation of the UV and X–ray solar observations can be particularly difficult and sometimes incomplete if based only on direct morphological analysis. Peres et al. (1987), Peres and Reale (1993), and Reale & Peres (1995) have proved that models of plasma confined in coronal loops can be useful to study the physical properties of the solar corona and they can be important in the interpretation of the observations, through the synthesis of the emission from such models and the subsequent comparison with EUV and X–ray observations of loops. The strategy suggested by such authors is illustrated in Fig. 1. One starts with a plausible grid of

Correspondence to: S. Orlando

loop models characterized by a set of values for the relevant physical parameters (e.g. loop geometry, temperature, plasma density, plasma velocity, etc.). From the grid of models the emission is synthesized in specific lines and bands of interest and folded with a specific instrument response. The resulting synthetic emission line distribution is then compared with that observed and such a detailed and quantitative comparison is used to constrain and/or derive the loop conditions most appropriate to fit the observations. The effectiveness of such a method has been first shown in the studies by Pallavicini et al. (1981) which showed the fundamental appropriateness of the hydrostatic loop model by Rosner, Tucker, and Vaiana (1978).

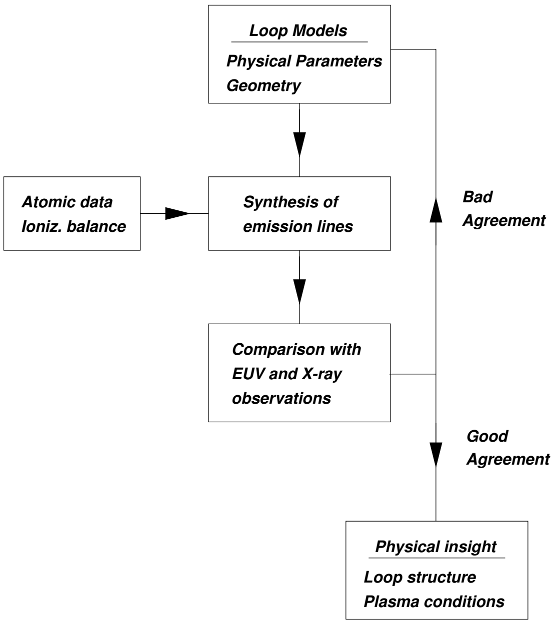

Fig. 1. The figure illustrates the various steps to be followed for deriving physical informations about emitting plasma comparing the emission line distribution synthesized from loop models with that observed.

In the light of the above considerations, we developed a detailed diagnostic tool comprising a siphon flow loop model which takes into account a wide set of physical effects and a tool to synthesize the emission lines from the model profiles which takes into account the non–equilibrium ionization effects important in the presence of a plasma flow through the steep gradient of the temperature in the transition region. In this paper, we apply the tool to two examples of loop hosting a subsonic flow and a shocked flow, respectively, to investigate the deviations from ionization equilibrium induced by the flows and we discuss their effects on the UV and EUV emission lines observed by CDS and SUMER.

Our paper is structured as follows: in Sect. 2 and in Sect. 3 we describe the siphon flow model adopted, the synthesis of the emission lines and the non–equilibrium ionization calculation, respectively; in Sect. 4 we discuss the effects of plasma flow on a set of UV and EUV lines observed by CDS and SUMER; finally, in Sect. 5 we draw our conclusions and the future prospects.

2 The model

We use the hydrodynamic steady–state siphon flow model formulated by Orlando, Peres, and Serio (1995a). The model assumes a semicircular loop of length 2L and cross–sectional area uniform along the loop hosting a stationary siphon flow (cf. Fig. 2). The model takes into proper accounts the effects of gravity, thermal conduction, radiative losses from an optically thin plasma, and local energy input; it is based on the fluid equations of mass, momentum, and energy conservation:

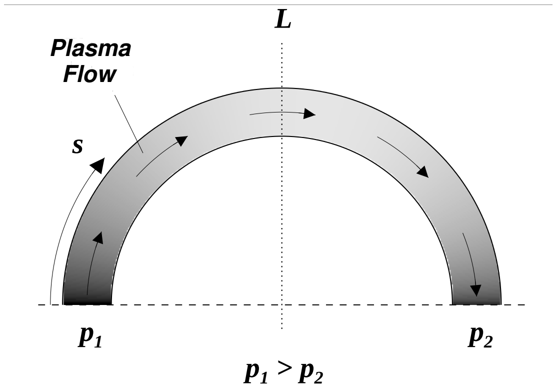

Fig. 2. Coronal loop geometry: s is the field lines coordinate, L is the loop semilength, and p_1 and p_2 are the plasma pressure values at the two loop footpoints, respectively.

$$\rho u = F_M \tag{1}$$

$$\rho u \frac{\partial u}{\partial s} = -\frac{\partial p}{\partial s} - \rho g_0 \cos\left(\frac{\pi s}{2L}\right) \tag{2}$$

$$\frac{u\rho^\gamma}{\gamma-1}\frac{\partial}{\partial s}\left(\frac{p}{\rho^\gamma}\right) - \frac{\partial}{\partial s}\left(\kappa\frac{\partial T}{\partial s}\right) = E_H - \frac{p^2}{4k_B^2T^2}\Lambda(T) \tag{3}$$

where $\rho = \mu m_H n_p$ is the plasma mass density, $\mu = 1.268$ is the mean atomic mass for solar abundances, m_H is the hydrogen atom mass, n_p is the proton number density, u is the bulk plasma velocity, F_M is the (fixed) mass flux, s is the field lines coordinate, $p = 2n_pk_BT$ is the plasma pressure, k_B is the Boltzmann constant, T is the plasma temperature, g_0 is the solar surface gravity, L is the loop semilength, $\gamma = 5/3$ is the ratio of the specific heats, $\kappa = 9.2 \times 10^{-7}T^{5/2}$ is the thermal conductivity in cgs units (Spitzer, 1962), E_H is the volumetric heating rate, and $\Lambda(T)$ is the radiative loss per unit emission measure (Raymond and Smith, 1977).

The fluid equations are solved choosing the lower boundary located at the base of the transition region where the temperature is 2×10^4 K and for different values of velocity, density and heat flux at the base of the upflowing leg. In order to achieve high reliability close to critical points, two independent numerical codes are used to solve the equations: the first one based on a fourth–order Runge–Kutta method with adaptive stepsize control and the second one on the Bulirsch–Stoer method (Press et al., 1986; Stoer and Bulirsch, 1980).

The numerical and physical accuracy of the model is very important when making detailed comparison with the observations.

Orlando, Peres, and Serio (1995a) explored systematically the solution space and identified four different classes of solutions: 1) subsonic solutions in which the plasma flow is subsonic along all the loop; 2) transonic solutions passing through the sonic point (where the flow velocity is equal to the local isothermal sound speed) which separate the loop in two branch one characterized by subsonic flow and the other by supersonic flow; 3) supersonic solutions in which the plasma flow is supersonic along all the loop; and 4) unphysical solutions which are not defined in all the loop and which are often double–valued.

3 Lines synthesis and non–equilibrium ionization

The analysis of solar UV and EUV observations, and in particular of spectral lines, is a powerful diagnostic tools for the physical conditions in the outer layers of the solar atmosphere, more specifically in the transition region and the lower corona. Since deviation from equilibrium ionization may have a non–negligible effect on the UV and X–rays lines, especially in those emitted from the transition region where the plasma moves through very steep gradient of temperature, it is crucial to take into account these effects on the interpretation of the solar observations.

In the light of the above considerations, we compute the density of each ion species of a given element along the loop taking into account the non–equilibrium ionization. We solve therefore a system consisting of the continuity equations of the ionization species of the elements considered. For steady state conditions, and for plasma bulk velocity parallel to the magnetic field lines, the system of continuity equations is:

$$\frac{d}{ds}(n_i u) = n_e \left[n_{i+1}\alpha_{i+1} + n_{i-1}S_{i-1} - n_i(\alpha_i + S_i) \right] \qquad (i = 1, ..., l) \quad (4)$$

where l is the maximum degree of ionization ($i = 1$ corresponds to the neutral element and $i = l$ corresponds to the element completely ionized), $n_e (= n_p)$ is the electron number density, n_i is the number density of the ion i, $\alpha(n_e, T)$ and $S(n_e, T)$ are the collisional–dielectronic recombination coefficients and the collisional ionization coefficients of Summers (1974) respectively, and where $\alpha_1 = S_0 = \alpha_{l+1} = S_l = 0$. The profiles of electron number density n_e, temperature T, and velocity u along the loop are known from the solution of the hydrodynamic equations (Eqs. 1–3). The radiative losses $\Lambda(T)$ used in Eq. 3 are computed in the approximation of ionization equilibrium. As discussed in Spadaro et al. (1990), even if the influence of taking into proper account the non–equilibrium ionization in the $\Lambda(T)$ may sometimes be significant, in those cases the global structure of loop models is influenced so little (less than 10%) that the effect on the ions density profiles is negligible.

Table 1. Emission lines selected

Ion	Wavelength (Å)	$\log T_{ion}$ (K)	Instruments
C II	1335.30	4.6	SUMER
O III	599.600	5.0	CDS
O IV	554.370	5.2	CDS
O V	629.730	5.4	SUMER & CDS
Ne VI	561.380	5.6	CDS
Ne VII	895.180	5.8	SUMER
Si VIII	1440.50	6.0	SUMER
Si XII	521.100	6.2	SUMER & CDS

We assume as boundary conditions that the plasma is in ionization equilibrium at the base of the upflowing leg ($s = 0$) as in Noci et al. (1989), Spadaro et al. (1990, 1995), and Peres, Spadaro, and Noci (1992):

$$(n_i)_{eq} S_i = (n_{i+1})_{eq} \alpha_{i+1} \qquad (i = 1, ..., l-1) \quad (5)$$

$$\sum_{i=1}^{l} (n_i)_{eq} = A_c n_p \quad (6)$$

where A_c is the abundance of the specific element relative to the hydrogen.

The density of the ion species n_i of the element considered are used to compute the intensity of the spectral lines predicted by our siphon flow model. The power emitted per cm^3 and per sr in a transition $j - k$ is given by (Kato, 1976; Stern, Wang, and Bowyer, 1978):

$$E_{jk} = \frac{1}{4\pi} n_i n_e C_{gj} W_{jk} B_{jk} \, , \qquad \mathrm{erg\ cm^{-3}\ s^{-1}\ sr^{-1}} \quad (7)$$

where n_i is the number density of the ions producing the line, W_{jk} is the energy involved in the transition $j - k$, B_{jk} is the radiative decay branching ratio, and C_{gj} is the collisional excitation rate, given by (Kato, 1976):

$$C_{gj} = 8.63 \cdot 10^{-6} \exp\left(\frac{-W_{gj}}{k_B T} \right) \frac{1}{\sqrt{T}} \left(\frac{\Omega_{gj}}{\omega_g} \right) \, , \ \mathrm{cm^3\ s^{-1}} \quad (8)$$

where Ω_{gj} is the effective collisional strength from the ground level and ω_g is the statistical weight of the ground level.

The detailed synthesis of loop emission in specific bands and lines are obtained with the use of ASAP, a powerful presentation system for astrophysical plasma models (Maggio et al., 1994).

4 Distributions of line emission along loops hosting stationary plasma flows

We used the method described in the above sections to investigate the possible observable effects that a stationary flow confined in a loop can induce on the distribution of UV lines emission along the magnetic flux tube as observed by CDS and SUMER. To this end, we selected a set of lines commonly used to analyze the physical conditions of the emitted plasma which form at temperatures ranging from the low transition region (C II with a temperature of maximum line formation $\log T(\mathrm{K}) = 4.6$) to the corona (Si XII with a temperature of maximum line formation $\log T(\mathrm{K}) = 6.2$) in order to study the effects of the flow at different temperature regimes. In table 1 we report the emission lines selected together with the maximum temperature of line formation T_{ion} and the SOHO instruments able to observe the line.

In the following sections, we discuss an example of coronal loop hosting a subsonic siphon flow (described by solutions of class 1 discussed in Sect. 2) and an example of loop hosting a transonic siphon flow undergoing a shock (described by solutions of class 2).

4.1 Subsonic siphon flow

To analyze the observable effects of a subsonic flow confined in a coronal loop on the emission lines listed in table 1, we considered a case characterized by the physical and geometrical parameters listed in table 2 as an example of solution obtained for a typical coronal loop. Fig. 3 shows the profiles of temperature, density and Mach number (defined as the ratio u/c_s, where c_s is the local isothermal sound speed) along the loop.

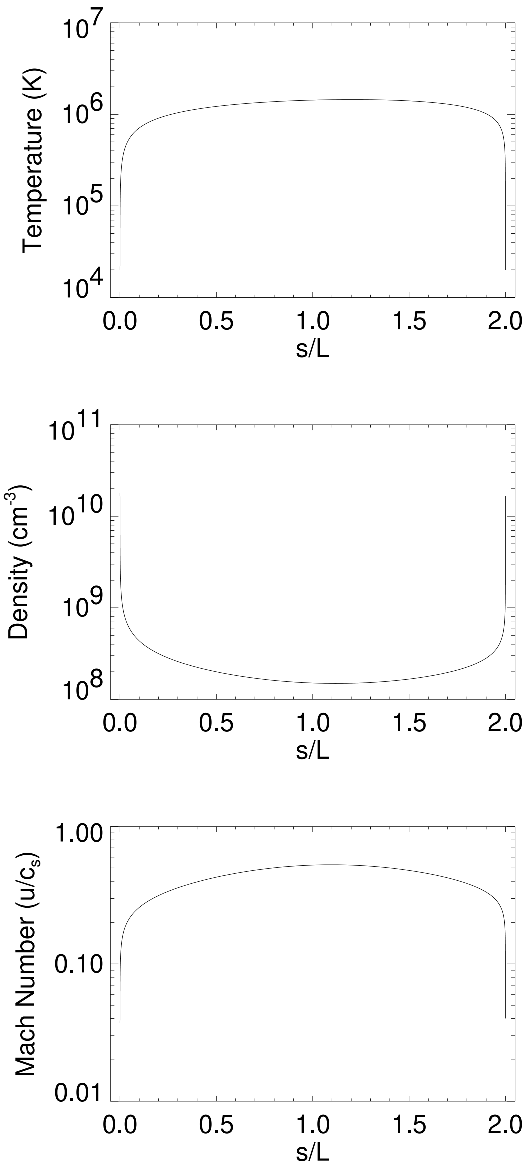

Fig. 3. The subsonic siphon flow model obtained for a typical coronal loop with the parameters listed in table 2. The figure reports the profiles of temperature T (top panel), density n_p (middle panel), and Mach number u/c_s (bottom panel) along the loop.

Table 2. Parameters characterizing the subsonic and the shocked siphon flow described in section 4.1 and 4.2. Variables are as follows: T_0, p_0, and u_0 are, respectively, the temperature, the pressure, and the velocity at the base of the upflowing leg, E_H is the volumetric heating rate (uniform along the loop), L is loop semilength, and T_{max} is the maximum of the temperature.

	Subsonic Sip. Flow	Shocked Sip. Flow
T_0 (K)	2.0×10^4	2.0×10^4
p_0 (dyn cm^{-2})	0.1	1.0
u_0 (cm s^{-1})	6.0×10^4	6.7×10^4
E_H (erg cm^{-3} s^{-1})	5.4×10^{-4}	2.6×10^{-2}
L (cm)	2.0×10^9	2.0×10^9
T_{max} (K)	1.4×10^6	2.6×10^6

Fig. 4 shows the distributions of surface brightness in the lines listed in table 1, computed from the model profiles of Fig. 3 and taking into account the non–equilibrium ionization effects induced by the plasma flow inside the loop as discussed in Sect. 3. Note that in the case of the lines forming in the transition region, the footpoints are brighter than the apex of the loop by several orders of magnitudes. Emission profiles with analogous large difference between footpoints and top are obtained from all the solutions with maximum plasma temperature $> 10^6$ K.

The figure shows that the effects of the plasma flow introduce a significant asymmetry of the distribution of emission along the loop. In particular, in the case of lines forming at the base of the transition region (e.g. C II 1335.3 Å, O III 599.6 Å) only the footpoint of the upflowing leg is visible, and, in general, for lines forming below 10^6 K the ascending branch is much brighter than the descending branch. On the other hand, in the case of lines forming in the corona, i.e. $\log T_{ion}(\mathrm{K}) > 6$, the descending branch is brighter than the ascending ones (cf. SI XII 521.1 Å line). From this example, we conclude that the effects of a subsonic siphon flow confined in a hot coronal loop should be in principle detectable by CDS and SUMER from the measured asymmetry in the distribution of the emission along the loop for these lines.

4.2 Shocked siphon flow

We have explored the effects that shocks can have on the distribution of the line emission along a coronal loop. Orlando, Peres, and Serio (1995b) explored systematically the conditions for the presence of stationary shocks in transonic (class 2 mentioned in Sect. 2) and supersonic (class 3 mentioned in Sect. 2) solutions in coronal loops. In the example sketched in Fig. 5, the flow starts subsonic at the base of the transition region and becomes supersonic at the sonic point i.e. where the bulk velocity is equal to the local isothermal sound speed.

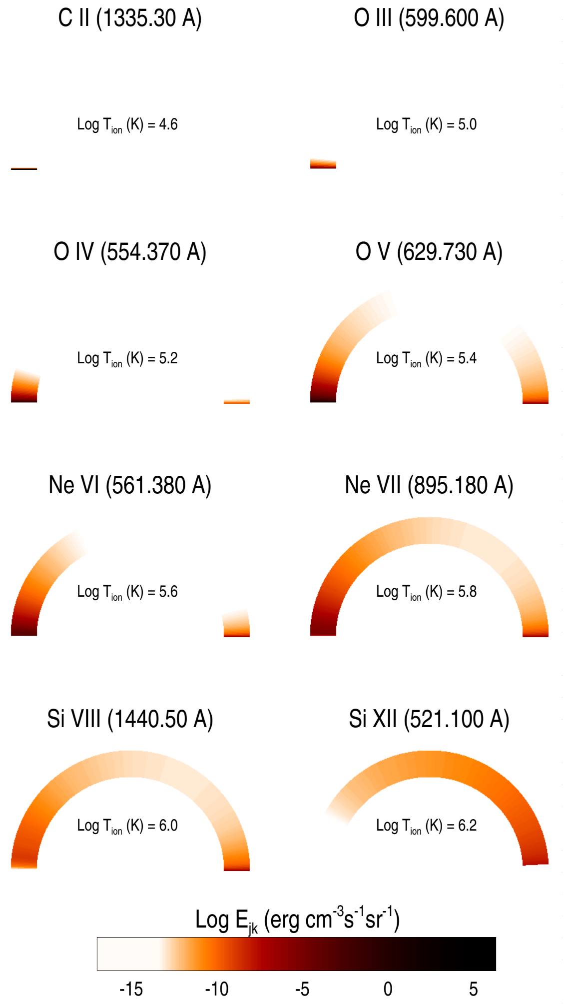

Fig. 4. Distribution of emission in logarithmic scale (black is bright, white is faint) in the lines listed in table 1 along the loop, computed from the results shown in Fig. 3, taking into account the non–equilibrium ionization effects.

Since the plasma flow has to stop, eventually, on reaching the solar surface at the other end of the loop, the descending supersonic plasma flow must undergo a shock before reaching the solar surface (this is the only way to match the two conditions).

Fig. 6 shows an example of transonic solution which undergoes an adiabatic shock and which is characterized by the physical and geometrical parameters listed in table 2. As for the subsonic siphon flow discussed before, we report in the figure the profiles of temperature, density, and Mach number along the loop. Note the adiabatic shock in the descending branch after the solution has reached the sonic point.

Fig. 7 shows the distribution of emission along the loop in the lines listed in table 1. The asymmetry of the brightness along the loop is particularly evident in the lines forming in the transition region for which, as in the previous example, the upflowing leg is much brighter than the downflowing leg. The presence of the shock is also evident as a sudden increase of emission in the transition region lines and as a sudden decrease of emission in the coronal lines.

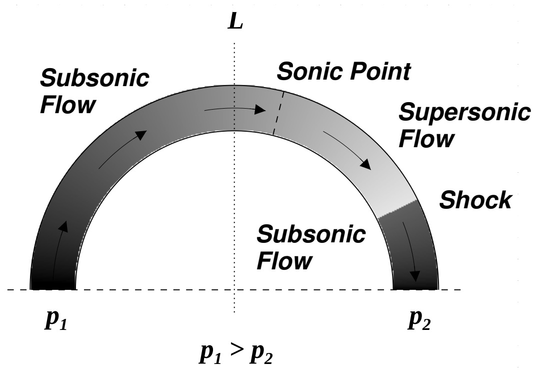

Fig. 5. Example of shocked siphon flow along a flux tube: the velocity increases monotonically, starting from the base of the upflowing leg, and becomes supersonic at the sonic point; then the flow undergoes a shock in the descending branch, reaching the solar surface at the other end of the loop with subsonic values of the velocity.

5 Conclusions

We have presented a detailed siphon flow loop model which can be used as a diagnostic tool to interpret solar UV and X–ray observations in specific bands and lines. The model is used to synthesize the emission lines taking into account the non–equilibrium ionization effects induced by the plasma flows through the steep gradient of temperature of the transition region.

We applied the tool to investigate the effects of plasma flow confined in coronal loops on a set of selected emission lines observed by CDS and SUMER, commonly used to analyze the physical conditions of the emitting plasma forming at temperature ranging from the base of the transition region to the corona, in order to analyze these effects at different temperature regimes.

We showed that the presence of the flow makes the distribution of emission in the lines significantly asymmetric especially in the transition region emission (for instance the O V 629.73 Å line) but also in the coronal emission (cf. Si XII 521.1 Å). Flows undergoing a shock produce very asymmetric distribution of the emission and the shock itself is particularly evident as a sudden increase of emission in the transition region lines and as a sudden decrease of emission in the coronal lines.

These results are important because CDS and SUMER have the angular resolution adequate to detect the loop asymmetries discussed before and, therefore, to show or to exclude the presence of siphon flow inside the hot coronal loops. Images with the adequate angular resolution are also crucial to derive the temperature stratification in the individual loop (through the analysis of emission lines forming at different temperatures) and then to estimate the other physical parameters of the plasma.

In the next future, we will apply the diagnostic tool presented here to analyze and interpret CDS and SUMER observations collected in November 1997 during an observa-

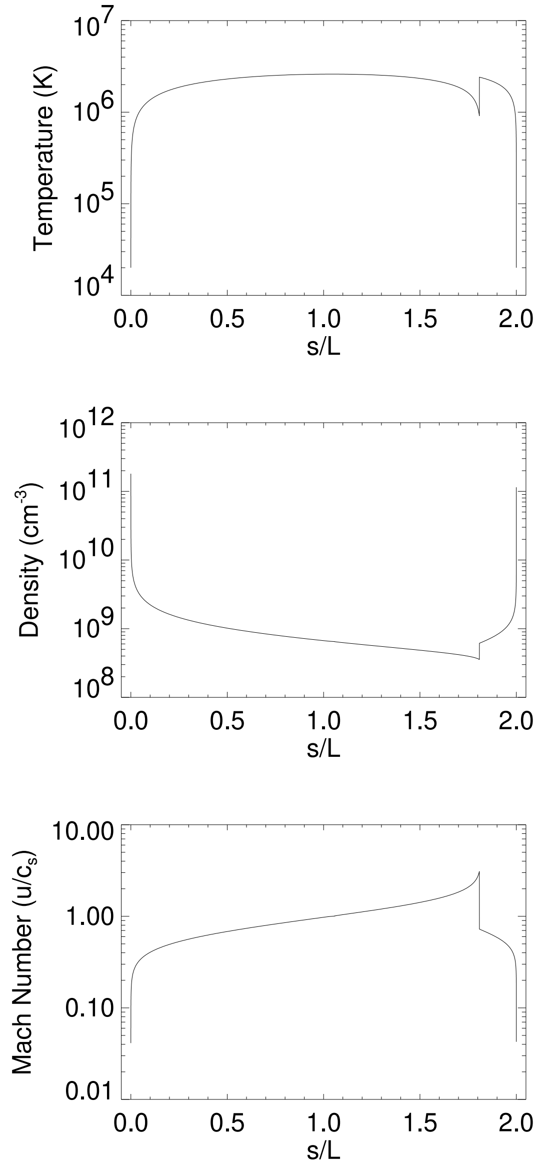

Fig. 6. As in Fig. 3, but for an example of shocked siphon flow characterized by the parameters listed in table 2.

tional campaign. The observational program was dedicated to study the hot stationary coronal loops and the EUV loops rooted in sunspots. As about the hot stationary coronal loops to which our tool is applicable, our task is to ascertain the loop structure and morphology, the physical conditions of the confined plasma and to get fundamental information on the temperature and density stratification.

Acknowledgements. We acknowledge useful criticisms and suggestions from an anonymous referee. This work was supported in part by European Space Agency and in part by Agenzia Spaziale Italiana and by Ministero della Università e della Ricerca Scientifica e Tecnologica.

References

Kato T. 1976, ApJS 30, 397
Maggio A., Reale F., Peres G., Ciaravella A. 1994, Comp. Phys. Com. 81, 105
Noci G., Spadaro D., Zappalà R.A., Antiochos S.K. 1989, ApJ 338, 1131
Orlando S., Peres G., Serio S. 1995a, A&A 294, 861
Orlando S., Peres G., Serio S. 1995b, A&A 300, 549
Pallavicini R., Peres G., Serio S., Vaiana G.S., Golub L., Rosner R., 1981, ApJ 247, 692
Peres G., Reale, F., Serio, S., Pallavicini, R., 1987, ApJ 312, 895
Peres G., Spadaro D., Noci G., 1992, ApJ 389, 777
Peres G., Reale, F., 1993, A&A 275, L13
Press W.H., Flannery B.P., Teukolsky S.A., Vetterling W.T. 1986, 'Numerical Recipes', (New York: Cambridge Univ. Press)
Raymond J.C., Smith B.W., 1977, ApJS 35, 419
Reale, F., Peres, G., 1995, A&A 299, 225
Rosner R., Tucker W.H., Vaiana G.S., 1978, ApJ 220, 643
Spadaro D., Zappalà R.A., Antiochos S.K., Lanzafame G., Noci G. 1990, ApJ 362, 370
Spadaro D., Orlando S., Peres G., Leto P. 1995, A&A 302, 285
Spitzer L., 1962, Physics of fully ionized gases. Wiley, New York
Stern R., Wang R., Bowyer S. 1978, ApJS 37, 195
Stoer J., Bulirsch R. 1980, In: 'Introduction to numerical analysis', (New York: Springer–Verlag)
Summers H.P. 1974, Internal Mem. 367, Astrophysics Research Div., Appleton Lab., Abingdon, Oxon

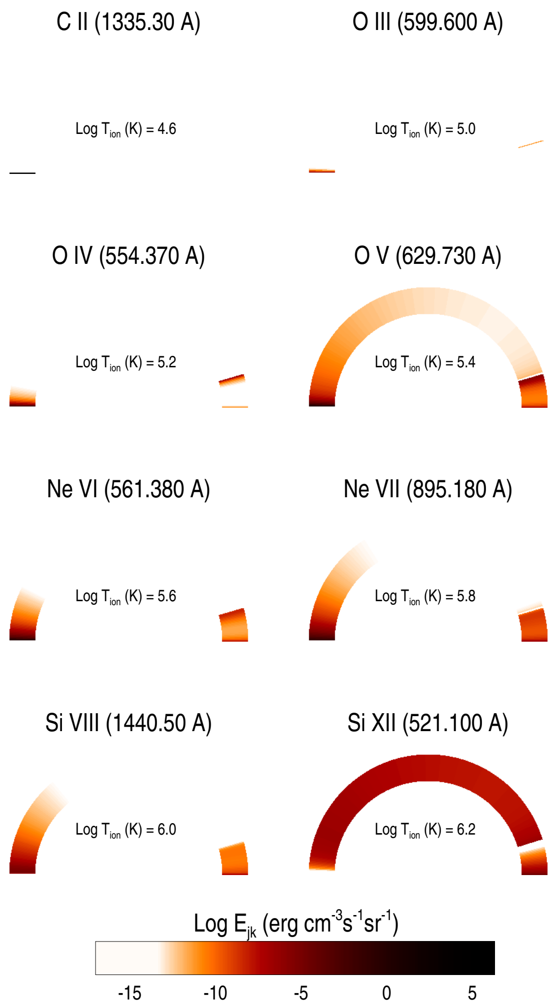

Fig. 7. As in Fig. 4, but for the shocked siphon flow presented in Fig. 6.